

Finite Element and Experimental Investigation of Piezoelectric Actuated Smart Shells

V. K. Gupta*

Engineering College, Kota 324 010, India

and

P. Seshu† and K. Kurien Issac‡

Indian Institute of Technology Bombay, Mumbai 400 076, India

In the recent years, research on the use of piezoelectric actuators for shape and vibration control of structures has been gaining prominence. Analytical and finite element models have been developed to analyze structures under piezoelectric actuation, but experimental studies, particularly on curved structures, are limited. In the current study, a finite element model is developed for piezoelectric actuated shell structures, based on Ahmad's reduced shell element. Experiments have been conducted on a number of structures like straight beams, curved beams, and shells. Finite element and experimental results have been shown to match well. Nonlinear behavior has been observed in the experiments, particularly at higher fields, and complete hysteresis loops have been presented. The finite element is then applied to the study of deformation of a typical paraboloid shell (representative antenna shell) under piezoelectric actuation. It has been shown that piezoelectric actuation can be used to induce desired deformation shapes in the antenna shell, which result in beam steering and shaping.

Nomenclature

$[B]$	= strain matrix
d_{31}, d_{32}	= piezoelectric strain coefficient
I	= moment of inertia
K	= stiffness
ℓ, m, n	= direction cosines
N	= shape function
$[T_\varepsilon]$	= transformation matrix
t_i	= thickness of node i
$\{u, v, w\}$	= linear displacements
V	= applied voltage
$\{V_j\}$	= normal vector along direction j
$\{x, y, z\}$	= Cartesian coordinates
Y	= Young's modulus of elasticity
$\{\alpha, \beta\}$	= rotations along x and y axes
ε	= strains
ξ, η, ζ	= curvilinear coordinates
ρ	= density
σ	= stresses
ϕ	= electric field

Subscripts

i	= node i
p	= piezoactuator
s	= substructure

I. Introduction

VARIOUS theoretical models have been developed by researchers to study the effect of piezoelectric actuation on beams, plates, and shells.¹⁻⁷ Piezoelectric materials are normally assumed to be linear, and the actuation strain is modeled like a thermal strain. The constitutive relations are based on the assumption that the total strain in the actuator is the sum of the mechanical strain induced by any stress, thermal strain as a result of any temperature and the controllable actuation strain as a result of electric voltage.

Several finite element models have been suggested for modeling piezoelectric actuation of beams and plates⁸⁻¹⁴ and shells.¹⁵⁻²¹ Hwang and Park,¹⁰ considered one electric degree of freedom per element to consider electromechanical coupling, whereas Chen et al.¹² considered one electric degree of freedom per node. Gaudenzi and Bathe²² presented an iterative finite element procedure for the coupled electroelastic analysis of two- and three-dimensional piezoelectric continua. Lin et al.²³ included effect of adhesive layer by using an eight-node quadratic isoparametric element for plate and 16 node-adhesive interface elements.

Thirupathi et al.¹⁷ used Ahmad et al.'s²⁴ laminated quadrilateral shell element with eight nodes for the finite element formulation. They carried out explicit integration in thickness direction. Piezoelectric actuation was modeled as an initial strain. Chen et al.^{19,20} used eight-node, 40-degree-of-freedom finite element for vibration and shape control of shell structure containing an integrated distributed piezoelectric sensor and actuator. Reduced integration was used by them to improve performance of the element. A survey of various piezoelectric shell finite elements is given in Benjeddou,²⁵ where it was reported that only a few shell elements were found in literature.

Several studies reported comparison of theoretical and experimental results on straight beams and flat plates. Crawley and Anderson² reported good comparison (error ranging from 0.5% to 20%) of their theoretical model with experiments on aluminum, glass/epoxy, and graphite/epoxy beams. Varadan et al.²⁶ conducted experiments on cantilever beams and frames in the form of Y and T beams. Yang and Lee²⁷ conducted analytical and experimental studies on the vibration characteristics of a cantilever beam with a surface-bonded piezoelectric actuator. Shen²⁸ developed one-dimensional theory for the vibration analysis of beams containing piezoelectric sensors and actuators. Experiments were conducted on cantilever beam, and good agreement between experimental and theoretical results was found. Brennan and McGowan²⁹ carried out

Presented as Paper 2002-1362 at the AIAA/ASME/ASCE/AHS/ASC 43rd Structures, Structural Dynamics, and Materials Conference, Denver, CO, 22-25 April 2002; received 19 November 2003; revision received 30 April 2004; accepted for publication 13 May 2004. Copyright © 2004 by the American Institute of Aeronautics and Astronautics, Inc. All rights reserved. Copies of this paper may be made for personal or internal use, on condition that the copier pay the \$10.00 per-copy fee to the Copyright Clearance Center, Inc., 222 Rosewood Drive, Danvers, MA 01923; include the code 0001-1452/04 \$10.00 in correspondence with the CCC.

*Senior Lecturer, Mechanical Engineering Department, Akelgarh; guptavkr@sify.com.

†Associate Professor, Mechanical Engineering Department, Powai; seshu@me.iitb.ac.in.

‡Associate Professor, Mechanical Engineering Department, Powai; kurien@me.iitb.ac.in.

experiments on cantilever beam with a tip mass. They also stated that piezoelectric properties (e.g., capacitance) reveal a nonlinear behavior. Dhage³⁰ studied strain transfer behavior of piezoelectric actuator bonded on cantilever beam experimentally and theoretically. Effect of different bonding materials was studied, and it was found that cyano-acrylate-based bonding material was the best from an induced strain point of view. Clark et al.³¹ experimentally verified the analytical models developed in Dimitriadis et al.⁵ for distributed vibration excitation of thin plates. Single- and multiple-actuator excitation cases were considered. The correlation between the theoretical model and the experiment was found to be 20% at worst but around 5% in most cases. Literature on experiments conducted on curved structures is very limited.

Gupta et al.³² discussed results of the finite element model and experimental investigation on a curved beam. In this paper, the study is extended to shell structures. Finite element formulation for general shell structures is presented. Results of extensive experimental studies made on straight and curved beams and doubly curved shells with single and multiple actuators are discussed. In the end, finite element analysis of a smart paraboloid antenna shell containing piezoelectric actuators is discussed.

II. Shell Finite Element

A. Geometry

Figure 1 shows the reduced shell element. Three coordinate frames are used as shown in the figure:

- 1) Here x, y, z represents the global Cartesian coordinate frame.
- 2) The ξ, η, ζ is curvilinear coordinate frame defined for each element. Curvilinear coordinates and Cartesian coordinates are related using shape functions and coordinates in this curvilinear frame vary from -1 to 1 .
- 3) The x'_i, y'_i, z'_i is the local Cartesian coordinate system defined at each node, with z'_i being normal to the shell. x'_i and y'_i are tangential to the shell. The local x'_i axis is chosen to be perpendicular to the local z'_i axis and global y axis, unless the latter two are parallel. In

that case, x'_i is chosen to be perpendicular to local z'_i axis and global z axis.

V_{1i}, V_{2i} , and V_{3i} are unit vectors along x'_i, y'_i , and z'_i directions, respectively (Fig. 2). V_{1i} and V_{2i} are used to define the directions of nodal rotation degree of freedom (DOF) (α_i and β_i) shared by all elements at that node i . Each node on the reduced shell element has five degrees of freedom, three nodal displacements (u, v, w), and two rotations (α, β).

The coordinate of any point on the structure is given by

$$\begin{Bmatrix} x \\ y \\ z \end{Bmatrix} = \sum_{i=1}^8 N_i \begin{Bmatrix} x_i \\ y_i \\ z_i \end{Bmatrix} + \sum_{i=1}^8 N_i \xi \frac{t_i}{2} \begin{Bmatrix} \ell_{3i} \\ m_{3i} \\ n_{3i} \end{Bmatrix} \quad (1)$$

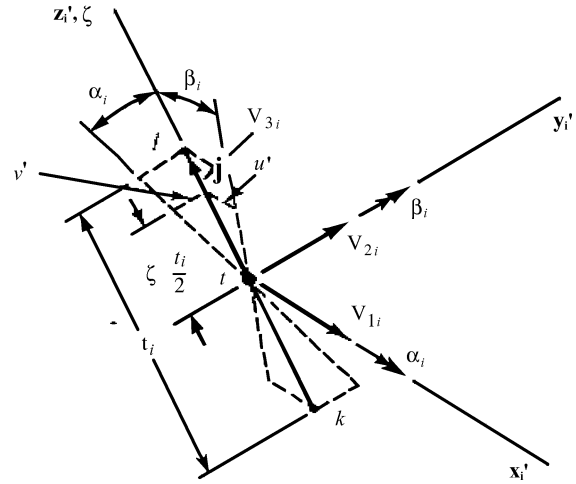


Fig. 2 Nodal vectors.

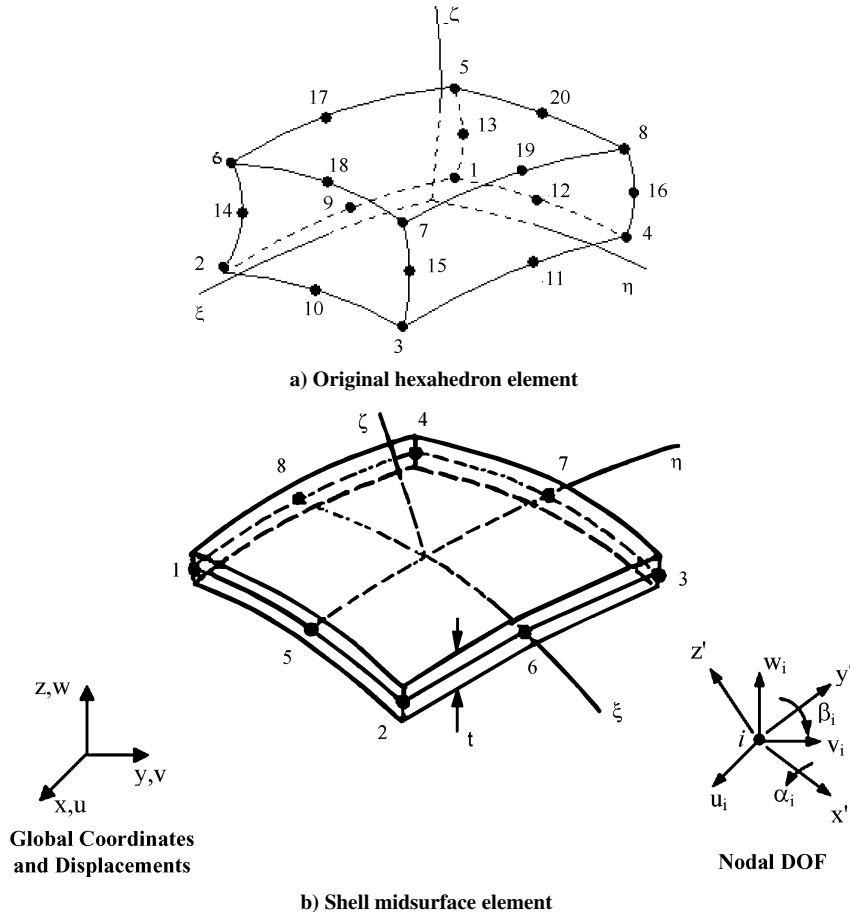


Fig. 1 Eight-noded degenerated shell element.²⁴

where $\ell_{3i}, m_{3i}, n_{3i}$ are the direction cosines of the normal to the surface at node i .

Displacement at any point in the shell element is given by

$$\begin{Bmatrix} u \\ v \\ w \end{Bmatrix}_{3 \times 1} = \sum_{i=1}^8 N_i \begin{Bmatrix} u_i \\ v_i \\ w_i \end{Bmatrix}_{3 \times 1} + \sum_{i=1}^8 N_i \zeta \frac{t_i}{2} [\mu_i]_{3 \times 2} \begin{Bmatrix} \alpha_i \\ \beta_i \end{Bmatrix}_{2 \times 1} \quad (2)$$

where

$$[\mu_i]_{3 \times 2} = \begin{bmatrix} -\ell_{2i} & \ell_{1i} \\ -m_{2i} & m_{1i} \\ -n_{2i} & n_{1i} \end{bmatrix} \quad (3)$$

where $\ell_{1i}, m_{1i}, n_{1i}$ are direction cosines of first tangential vector V_{1i} and $\ell_{2i}, m_{2i}, n_{2i}$ are direction cosines of the second tangential vector V_{2i} .

B. Strains and Stresses

Six strains in global direction are given by

$$\{\varepsilon\}_{6 \times 1} = [B]_{6 \times 40} \{u\}_{40 \times 1} \quad (4)$$

Strain matrix $[B]$ can be divided into two parts, one containing terms not related to ζ , that is, $[B_a]$, and the other containing terms proportional to ζ . Thus, $[B]$ can be written as

$$[B]_{6 \times 40} = [B_a]_{6 \times 40} + \zeta [B_b]_{6 \times 40} \quad (5)$$

Stress-strain relationship in local directions is given by

$$\{\sigma'\} = [Y'] \{\varepsilon'\} \quad (6)$$

where $\{\varepsilon'\} = [T_\varepsilon] \{\varepsilon\}$. $[Y']$ is the elasticity matrix in local coordinate frame.

C. Element Stiffness Matrix for Piezoelectric Actuated Shell

The element stiffness matrix is given by

$$[K]_{40 \times 40} = \int_V [B]_{40 \times 6}^T [T_\varepsilon]_{6 \times 6}^T [Y']_{6 \times 6} [T_\varepsilon]_{6 \times 6} [B]_{6 \times 40} dV \quad (7)$$

A typical piezoelectric shell element is shown in Fig. 3. It contains three layers, two piezoelectric (upper and lower) layers and one substructure layer. It is assumed that in-plane displacements (u' and v' in Fig. 2) vary linearly for points in piezolayers also and Eq. (2) is used to represent them. Material properties of piezoelectric material differ from the properties of the substructure and hence are not a continuous function of ζ . Hence the layered theory as proposed by Panda and Natarajan³³ is applied to consider the effect of different layers. Integration limit is split through each layer, by modifying the variable ζ to ζ_k in any k th layer such that ζ_k varies from -1 to $+1$ in that layer as shown in Fig. 4.

The change of variable is obtained from

$$\zeta = -1 + \frac{1}{t} \left[-h_k(1 - \zeta_k) + 2 \sum_{j=1}^k h_j \right] \quad (8)$$

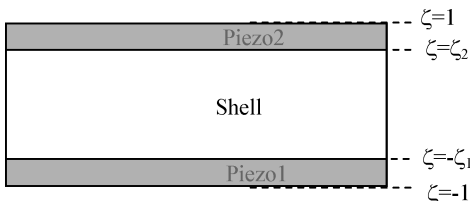


Fig. 3 Piezoelectric shell element.

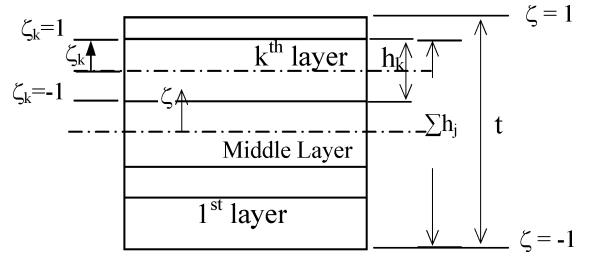


Fig. 4 Layered structure.

and $d\zeta = (h_k/t) d\zeta_k$. Here h_k is the thickness of k th layer and t is the total thickness of the structure.

Thus, the stiffness matrix is now

$$[K] = \sum_{k=1}^n \int_{-1}^1 \int_{-1}^1 \int_{-1}^1 ([B_a] + \zeta [B_b])^T [Y_k] \times ([B_a] + \zeta [B_b]) \frac{h_k}{t} |J| d\xi d\eta d\zeta_k \quad (9)$$

where n is the total number of layers and $|J|$ represents the determinant of the Jacobian.

In the case of piezoelectric actuation considered here, there are three layers. The integration in the ζ direction can be divided into three parts from -1 to $-\zeta_1$ (for lower piezoelectric material), $-\zeta_1$ to ζ_2 (for structure material), and ζ_2 to 1 (for upper piezoelectric material) for those elements where piezoelectric actuator is mounted (Fig. 3). For the rest of the elements, it can be integrated from -1 to 1 for structure material. For the case of symmetrically placed paired actuators,

$$\zeta_1 = \zeta_2 = t_s/(t_s + 2t_p) \quad (10)$$

where t_s and t_p are the thicknesses of the structure and piezoelectric actuator, respectively. It is assumed that symmetrically placed pair of actuators (i.e., on either side of shell midsurface) are used in the further development of the formulation, and hence the present element is strictly applicable to only such situations.

The stiffness matrix given in Eq. (9) can be written as

$$[K] = \int_{-1}^1 \int_{-1}^1 \int_{-1}^1 ([B_a] + \zeta [B_b])^T [Y_p] \times ([B_a] + \zeta [B_b]) |J| \frac{t_p}{t} d\xi d\eta d\zeta_{p1} + \int_{-1}^1 \int_{-1}^1 \int_{-1}^1 ([B_a] + \zeta [B_b])^T [Y_s] ([B_a] + \zeta [B_b]) |J| \frac{t_s}{t} d\xi d\eta d\zeta_s + \int_{-1}^1 \int_{-1}^1 \int_{-1}^1 ([B_a] + \zeta [B_b])^T [Y_p] \times ([B_a] + \zeta [B_b]) |J| \frac{t_p}{t} d\xi d\eta d\zeta_{p2} \quad (11)$$

where $\zeta_{p1}, \zeta_s, \zeta_{p2}$ are the changed variables [using Eq. (8)] for lower piezolayer, substructure and upper piezolayer, respectively; and $[Y_p]$ and $[Y_s]$ are elasticity matrices for piezoelectric and substructure materials, respectively. Numerical integration of the $[K]$ matrix is done in all three directions.

D. Forces Caused by Piezoelectric Actuation

Figure 5 shows a shell structure under piezoelectric actuation. It is assumed that the actuator is perfectly bonded to the structure (i.e., adhesive/bonding layer is not modeled). When an electric field ($\phi = V/t_p$) is applied on piezoelectric actuator, a free piezostress ε_{pf} will act on the surface of actuator. This can be modeled as the initial strain problem, and the initial strain vector can be written

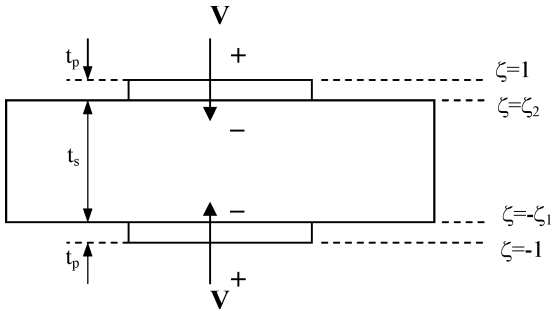


Fig. 5 Structure mounted with piezoelectric actuators.

as¹⁷

$$\begin{aligned} \{\varepsilon'_0\}^T &= \{\pm d_{31}\phi \quad \pm d_{32}\phi \quad \pm d_{33}\phi \quad 0 \quad 0 \quad 0\}^T \\ &\quad \text{for } \zeta_2 < \zeta < 1 \\ &= \{0 \quad 0 \quad 0 \quad 0 \quad 0 \quad 0\}^T \quad \text{for } -\zeta_1 < \zeta < \zeta_2 \\ &= \{\pm d_{31}\phi \quad \pm d_{32}\phi \quad \pm d_{33}\phi \quad 0 \quad 0 \quad 0\}^T \\ &\quad \text{for } -1 < \zeta < -\zeta_1 \quad (12) \end{aligned}$$

The direction of electric field vis a vis the poling direction decides the sign. If the electric field is applied in the direction of poling for an actuator, the initial strain will be positive (depending on the sign of d_{31}). The nodal loads caused by initial strain are given as

$$\{p_0\}_{40 \times 1} = \int_V [B]^T [T_\varepsilon]^T [Y'] \{\varepsilon'_0\} dv \quad (13)$$

On the same lines as Eq. (11), Eq. (13) can be written as

$$\begin{aligned} \{p_0\} &= \int_{-1}^1 \int_{-1}^1 \int_{-1}^1 [[B_a] + \zeta [B_b]]^T [T_\varepsilon]^T [Y_p'] \{\varepsilon_{pf1}\} \frac{t_p}{t} |J| \\ &\quad \times d\xi d\eta d\zeta_{p1} + \int_{-1}^1 \int_{-1}^1 \int_{-1}^1 [[B_a] + \zeta [B_b]]^T \\ &\quad \times [T_\varepsilon]^T [Y_p'] \{\varepsilon_{pf2}\} \frac{t_p}{t} |J| d\xi d\eta d\zeta_{p2} \quad (14) \end{aligned}$$

where ε_{pf1} and ε_{pf2} are free piezostains in the lower and upper piezoactuators, respectively, as defined in Eq. (12). Equation (14) is numerically integrated in all three directions using the Gauss-quadrature rule to obtain the force vector. This force vector is finally assembled to get overall force vector $\{F\}$. After assembly, the structure-level equation becomes

$$[K]\{\delta\} = \{F\} \quad (15)$$

which has been solved using Cholesky's factorization technique in order to obtain the deflections. It is reiterated here that in $\{\delta\}$ the translational displacements are along global x , y , z axes, but the rotations are along local axes x' , y' , z' .

III. Verification of Finite Element Formulation

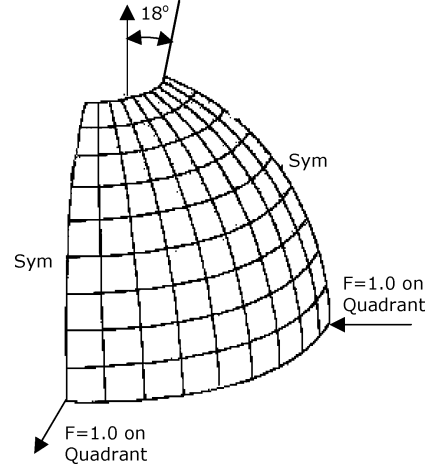
To verify the finite element model (FEM) formulation, initially, standard shell problem without piezoelectric actuation is solved, and then problems with piezoelectric actuation are solved. Experimental verification of FEM results is discussed subsequently.

A. Shell Structure Under External Forces

A typical doubly curved shell-type structure proposed by MacNeal and Harder³⁴ has been analyzed (Fig. 6). The original shell given by Morley³⁵ does not contain the 18-deg center hole, and hence MacNeal and Harder³⁴ modified the results of Morley³⁵ to take care of center hole. They also obtained FEM results using an eight-noded six-DOF (three translations and three rotations) QUAD8 element.³⁶

Table 1 Comparison of the normalized deflection for the hemispherical shell

Mesh	QUAD8 ³⁴	Present FE results	% Difference
2 × 2	0.025	0.140	460
4 × 4	0.121	0.363	200
6 × 6	0.494	0.953	92.9
8 × 8	0.823	0.986	19.8
10 × 10	0.955	0.994	4.1
12 × 12	0.992	0.995	0.3

Fig. 6 Hemispherical shell ($R = 10$ m; $t = 0.04$ m) (Ref. 34).

Selective reduced integration was used by them. In the present study, eight-noded reduced shell element with five-DOF (three translations and two rotations) has been used. Fully reduced integration has been carried out in the present study.

Current FEM results are compared with the FEM results given by MacNeal and Harder³⁴ and are summarized in Table 1. Both of these results are deflections normalized with respect to modified theoretical results of Morley.³⁵ It is observed that present FEM gives a normalized deflection of 0.995 (an error of 0.5%) with a 12×12 mesh and converges faster than MacNeal and Harder.³⁴

B. PVDF Bimorph

Figure 7 shows a bimorph beam [two polyvinylidene fluoride (PVDF) layers of opposite polarity bonded together] analyzed by Hwang and Park¹⁰ using a four-noded discrete Kirchhoff quadrilateral plate element with 12 structural DOF and one electrical DOF. Five elements (along the length) are taken for comparison (same as the number taken by Hwang and Park), and results are plotted in Fig. 8. It is observed that the current FEM results are in close agreement (maximum 1.5% deviation) with the results obtained by Hwang and Park.¹⁰

IV. Experimental Setup and Specimens

Experiments have been conducted to verify the FE formulation and to study behavior of structures under piezoelectric actuation. Variety of structures like beams (straight and curved) and doubly curved shells are experimentally tested.

A curved beam specimen with bonded piezoelectric actuators, along with typical equipment/instruments, used is shown in Fig. 9. An electric field is supplied to the actuator by a piezoamplifier (EPA-104-230 of Piezo System, Inc.[§]), the drive power source for the piezoelectric actuators. It is a high-voltage (200 V) and low-current (200 mA) power amplifier. The deflection caused by piezoelectric actuation is measured using a noncontact fiber-optic (FO) displacement sensor (RC-169 of Philtec, Inc.[¶]).

[§] Data available online at <http://www.piezo.com> [cited 20 Feb. 2002].

[¶] Data available online at <http://www.philtec.com> [cited 20 Feb. 2002].

Table 2 Properties of specimens

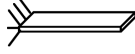
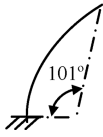
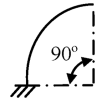
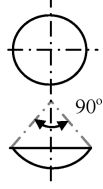
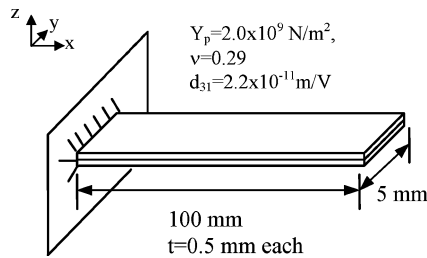
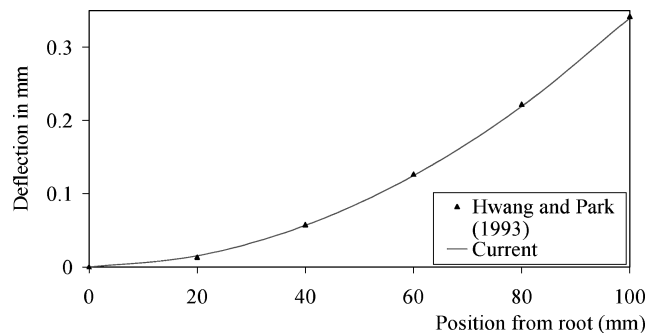
	Straight beam	Parabolic curved beam	Circular curved beam	Spherical shell
Property details				
Material	Al	Al	Al	Al
Modulus of elasticity, N/mm ²	0.638×10^5	0.638×10^5	0.638×10^5	0.530×10^5
Cantilever length l , mm	300	Focal length = 151, $\theta = 101$ deg	$R = 178$, $\theta = 90$ deg	$R = 203$, $2\theta = 90$ deg
C/s dimension ($w \times t$), mm	26×0.645	24.5×0.250	25.9×1.855	—
Density, kg/m ³	2689.4	2690	2721.7	2698.6

Table 3 Properties of piezoelectric actuator

Composition	SP-5H ^a	PSI-5A-S4-ENH ^b
Piezoelectric strain coefficient $d_{31} = d_{32}$, m/V	-265×10^{-12}	-190×10^{-12}
C/s dimension $b \times t$, mm	25.4×0.250	23.8×0.267
Elastic modulus $Y_1 = Y_2$, N/mm ²	4.76×10^4	6.6×10^4
Maximum voltage to be applied before depolarization V_{\max} , V	50 opposite to poling direction 150 along poling direction	90 opposite to poling direction 250 along poling direction

^aData available online at <http://www.sparklceramics.com>.^bData available online at <http://www.piezo.com>.**Fig. 7 Piezoelectric bimorph¹⁰** ($Y_b = 2 \times 10^{11}$ N/m², $\nu_b = 0.3$, $Y_p = 0.66 \times 10^{11}$ N/m², $\nu_p = 0.31$, $d_{31} = 190 \times 10^{-12}$ m/V, $V = 90$ V).**Fig. 8 Deflection of bimorph beam** ($Y_b = 2 \times 10^{11}$ N/m², $\nu_b = 0.3$, $Y_p = 0.66 \times 10^{11}$ N/m², $\nu_p = 0.31$, $d_{31} = 190 \times 10^{-12}$ m/V, $V = 90$ V).

Experiments have been conducted on straight and curved beams. The various specimens used in the experiment are shown in Figs. 10–12, and their properties are listed in Table 2.

A. Specimen Preparation and Experimental Determination of Properties

Figure 13 shows the sectional view of a straight beam with piezoelectric actuators mounted on top and bottom. Nonconductive adhesive (shown by paired hatch line) is used to mount the actuators on the beam structure. Both the surfaces of the actuators are fully elec-

troded. To access the lower (inner) surface of the actuators, metal shim electrodes are attached using conductive epoxy.

The Young's modulus Y of the material of the bare beam is estimated by experimental determination of the fundamental frequency of the beam and using the following relation³⁷:

$$\omega_{n1} = (3.516/L^2)\sqrt{YI/\rho A} \quad (16)$$

where A is the cross-sectional area of the beam and L is the cantilevered length of the beam. Based on the least counts of all of the instruments used in all measurements, possible error in the determination of the Young's modulus is estimated to be about 1.8%. Lightweight aluminum alloy is taken for straight and curved beams and shells. The Poisson's ratio is assumed to be 0.3 for all cases. The d_{31} -type lead zirconate titanate (PZT) actuators are chosen for the current study. Piezoceramic actuators manufactured by Piezo System, Inc.,** and Sparkler Ceramics, India,^{††} are chosen for experiments. The properties of the piezoceramic actuators are summarized in Table 3.

V. Deformation of a Straight Beam Under Piezoelectric Actuation

A. Straight Beam Mounted with One Pair of Actuators

Experiments are conducted to analyze deflection behavior of a straight beam (Fig. 14) under piezoactuation. Material properties for this beam correspond to straight beam in Table 2. The actuators used are PSI-5A-S4-ENH, properties of which are given in Table 3.

Deflections are measured at different points along length of the beam by moving the FO probe. FO probe is first moved along the length of beam without actuation and then with actuation. The difference in the two values (without actuation and with actuation) gives the deflection at a particular point. The results for an applied voltage of 90 V are plotted in Fig. 15.

Location of actuator is shown by region AB on the deflection curve. Theoretical results by Crawley and Anderson² are also plotted

**Data available online at <http://www.piezo.com> [cited 20 Feb. 2002].

^{††}Data available online at <http://www.sparklceramics.com> [cited 20 Feb. 2002].

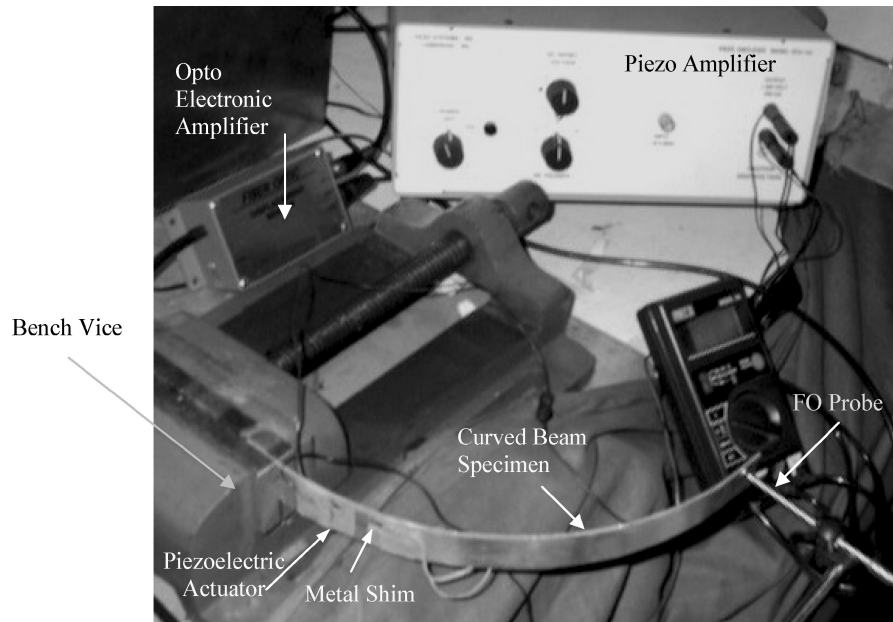


Fig. 9 Experimental setup for static response of a cantilever curved beam with bonded piezoelectric actuators.

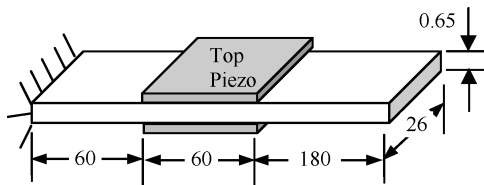


Fig. 10 Straight beam (dimensions in millimeters).

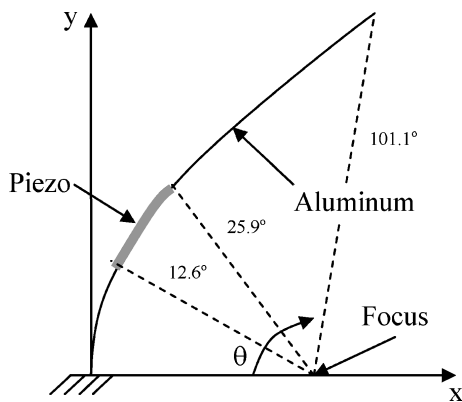


Fig. 11 Parabolic curved beam (dimensions in millimeters).

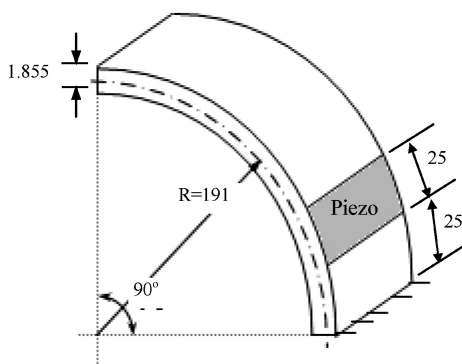


Fig. 12 Circular curved beam (dimensions in millimeters).

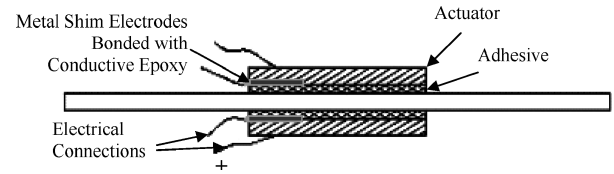


Fig. 13 Structure with bonded piezoelectric actuators.

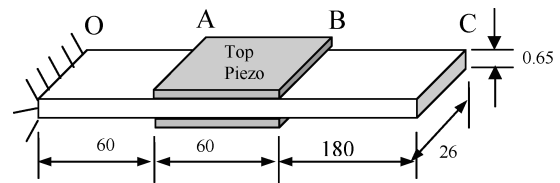


Fig. 14 Straight beam for study of end-moment actuator model (dimensions in millimeters).

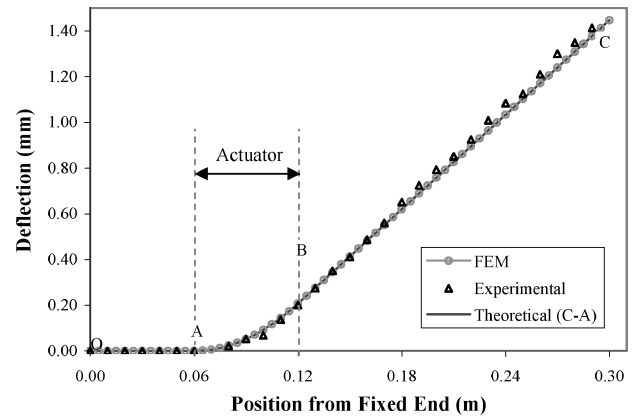


Fig. 15 Deflection along the length of cantilever beam under piezoactuation.

for comparison. FEM and theoretical (Crawley–Anderson) results are in perfect match. Deflection in the region OA is zero as no actuator effect comes into picture in this region. Deflection in the region AB is nonlinear because of the presence of the actuator. Region BC (starting from the farther end of actuator to the tip of beam) exhibits linear variation. A deviation of about 10% is observed between FEM and experimental values at the tip. The percentage deviation is estimated with the FEM value as reference.

B. Straight Beam Mounted with Multiple Actuators

To analyze the deformation pattern under multiple actuators, experiments are conducted on a straight beam mounted with two pairs of actuators (SP-5H) at different locations (Fig. 16). Material properties for this beam correspond to straight beam in Table 2 except that the thickness of the beam is now 0.25 mm. The poling directions of both the actuators are same. Actuator 1 is supplied 100 V while actuator 2 is supplied 100 V in the reverse direction. Deflections along the length are measured following the same procedure as in the preceding case.

Deflections with respect to distance from the fixed end are plotted in Fig. 17. The deflection curve can be divided into five regions: region OA, before the first actuator starts; AB, position of first actuator; BC, from the end of first actuator to start of second actuator; CD, position of second actuator; and DE, the region after second actuator. It is observed from the FEM results that the starting region where no actuator is present has zero deflection, whereas in the region where actuators are present that is, AB and CD have a non-linear variation of deflection. The region after the second actuator (i.e., DE) as well as the region between the actuators (i.e., BC) have a linear variation in deflection as expected. It is observed that the

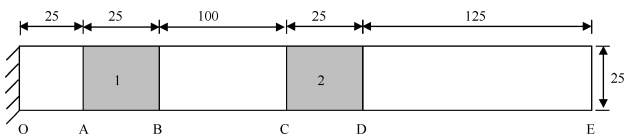


Fig. 16 Straight beam with two pairs of actuators.

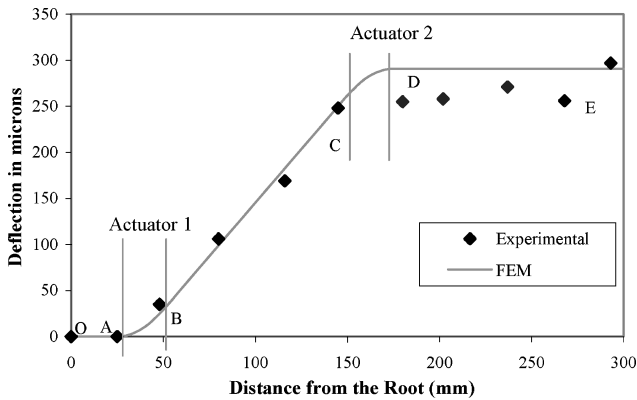


Fig. 17 Effect of multiple actuators on cantilever beam ($V_1 = -V_2 = 100$ V).

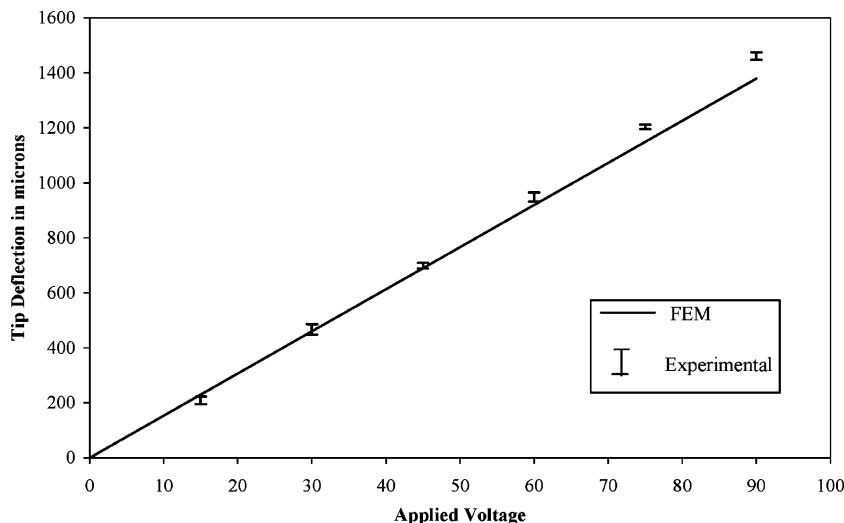


Fig. 18 Variation of deflection with voltage for straight beam.

FEM and experimental results are in close agreement (at worst 15% while in most cases <5% difference). The second actuator, supplied with the equal voltage supplied to the first actuator in reverse, attempts to annul the deflection caused by the first actuator. Hence the second actuator nullifies the effect of the first actuator, and the deflection curve is almost horizontal.

Thus, by using multiple actuators and adjusting voltages supplied to these actuators, it appears possible to obtain desired shape of the beam.

VI. Dependence of Deflections on Applied Voltage for Straight and Curved Beams

A. Unidirectional Variation of Voltage

Effect of voltage variation on piezoelectric actuation is analyzed by varying the voltage from 0 to the maximum permitted voltage V_{max} . Experiments are repeated a number of times in each case, and the variation in experimental results for one case is represented in Fig. 18. Very good repeatability (standard deviation to mean ratio <5%) has been observed. Results are summarized here for different specimens.

Experiments are first conducted on a straight beam (Fig. 10) mounted with piezoelectric actuators (PSI-5A-S4-ENH) using cyano-acrylate adhesive. Variation of tip deflection with applied voltage, determined experimentally and with FEM, is plotted in Fig. 18. FEM and experimental results show a maximum deviation of 7% at 90 V, but this is only 0.3% at 45 V. For the parabolic curved beam with SP-5H actuator, shown in Fig. 11, deviation between FEM and experimental results is 2.5% at 50 V and 13% at 25 V (Fig. 19). For the circular curved beam (with PSI-5A-S4-SNH actuator mounted) shown in Fig. 12, comparison of experimental result with FE prediction is plotted in Fig. 20. FEM and experimental results show a maximum deviation of 25% at 88 V, but this is only 3.3% at 45 V.

It is observed that experimental results indicate a nonlinear variation of deflection with increase in applied voltage, whereas the FEM model is linear. Thus, the difference between FEM and experimental results increases with increase in voltage in general except for parabolic curved beam. To analyze nonlinear behavior, further experiments are conducted for cyclic variation of applied voltage. Results are discussed in the next section.

B. Cyclic Variation of Applied Voltage

To examine whether the nonlinearity is caused by hysteresis, the voltage is varied continuously from zero to V_{max} , V_{max} to zero, and then to $-V_{max}$ and finally from $-V_{max}$ to zero in steps of 20 V. At each voltage step, the structure is allowed to settle for a few seconds, and then the readings are noted. The process is repeated for several cycles. Figure 21 shows the hysteresis loops obtained for a circular

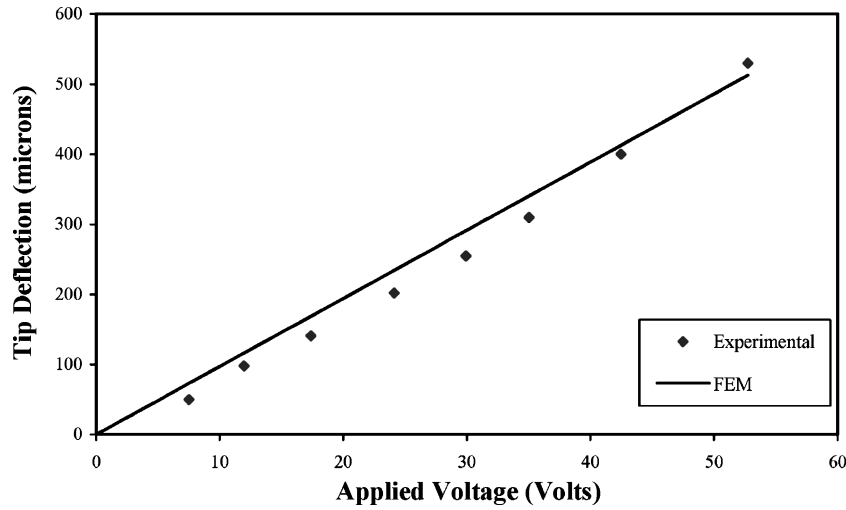


Fig. 19 Variation of deflection with voltage for parabolic curved beam.

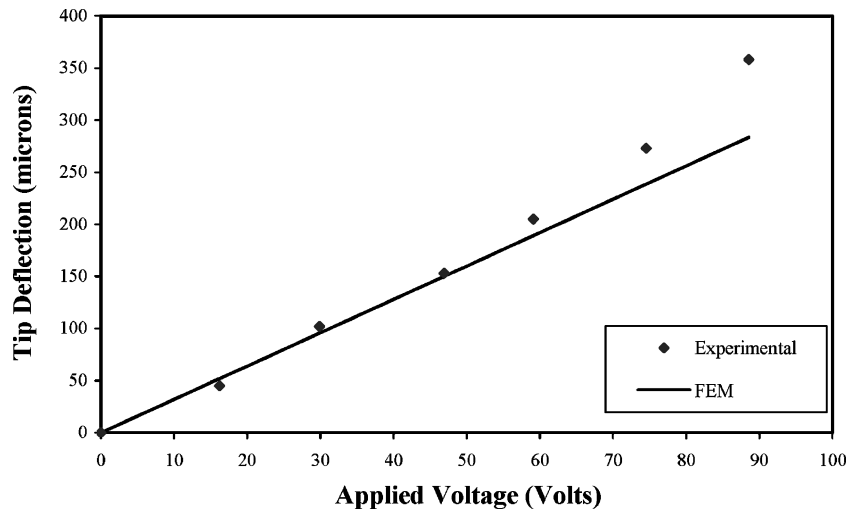


Fig. 20 Variation of deflection with voltage for circular curved beam.

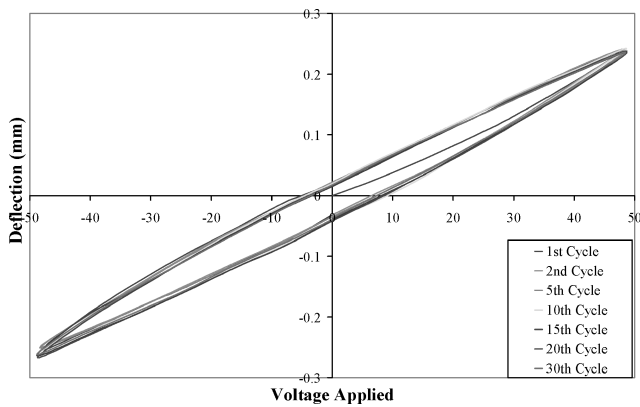


Fig. 21 Repeatability of hysteresis for circular curved beam.

curved beam over 30 cycles. It is observed that the system shows very good repeatability, and there is no shift in the hysteresis loops. The hysteresis loop is almost similar for specimens of different shapes (straight and curved beams) and different thickness (0.25–1.9 mm), and about 10% hysteresis is observed in all cases. Hysteresis is quantified as percentage ratio of the deflection at zero voltage to the maximum deformation achieved.²

C. Effect of Peak Voltage on Hysteresis Loop

Effect of peak voltage on hysteresis is studied by repeating the experimental cycle for different peak voltages ($\pm V_p$) on circular

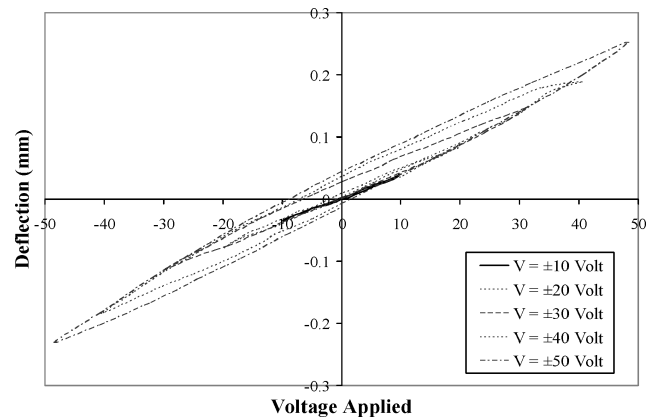


Fig. 22 Effect of peak voltage on hysteresis for circular curved beam.

curved beam. It is observed from Fig. 22 that the hysteresis increases with the increase in voltage and the minor loops are within the major loop.

VII. Experiments on Spherical Shell

To study the effect of piezoelectric actuation on shell structures, a spherical shell (shown in Fig. 23) is fabricated. The spherical shell was fabricated by making a die according to dimensions of the shell, and a press forming process was used to fabricate the shell. Because the sheet used was very thin, some wrinkles were formed on the

surface of the shell during fabrication. Coordinates of the different points on the fabricated shell surface were measured on an x - y coordinate measuring machine (having 0.01-mm accuracy). When a sphere was fitted through these points, an rms error of 5% in radius was obtained along radial direction. Actuators are mounted on the opposite edges at a distance of 50 mm from the apex on outer side of the shell (Fig. 24). Deflection is measured at point A (Fig. 24b), and results are compared with the present FEM results in Fig. 25 for the symmetric case, that is, both the actuators under the same electric field.

Figure 26 shows the variation of deflection around the circumference for the asymmetric case that is, when the two actuators are supplied with different voltages (one actuator is supplied 150 V and another 75 V). Here, the positive sign indicates that the shell is moving out while the negative sign indicates that the shell is moving in, at that particular point. It is observed that experimental results are in close match with the FEM results at many places. There is significant deviation between FEM and experimental results at some locations (maximum 20%) near the position of the wrinkles (A and B in Fig. 26), whereas deviation is less than 10% at other places.

VIII. Shape Control of Smart Antenna Shell

One of the application areas currently being actively pursued for piezoelectric actuation is the shape control of an antenna.^{38–40} The central idea is to apply suitable electric fields to the actuators, placed at appropriate locations on the antenna shell structure and induce the desired deformation of the antenna structure. These deformations, in turn, affect the path length of rays (phase difference) and hence the resulting radiation pattern. *Steering* refers to changing the principal direction of the antenna and is used when one wants to change the scanning area from one

location to another location (Fig. 27). *Shaping* refers to changing the area covered around the principal direction and is used when the area covered at a particular location is to be increased or decreased.

The finite element developed is now used to study the deformation pattern of a typical paraboloid smart antenna shell with four piezoelectric actuators (Fig. 28). It is assumed that the poling direction for all actuators is from the outside to the inside of the shell. Figure 29 depicts a typical finite element mesh used.

To study the deformation pattern of the shell, the following cases are considered:

- 1) All actuators are under the same field, that is, $V_A = V_B = V_C = V_D = 300$ V.
- 2) Pairs of actuators are under the opposing field, that is, $V_A = V_B = 300$ V, $V_C = V_D = -300$ V.

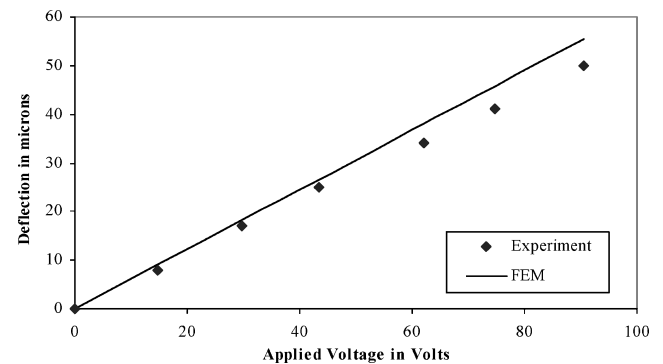


Fig. 25 Variation of deflection with applied electric field ($V_1 = V_2$).

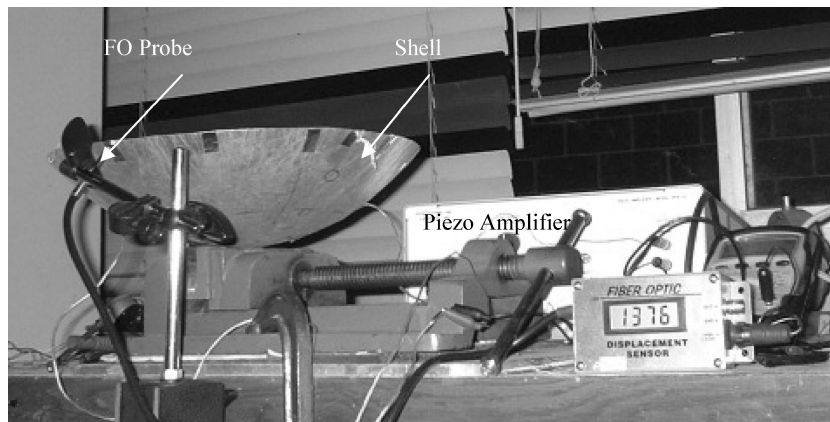


Fig. 23 Experimental setup.

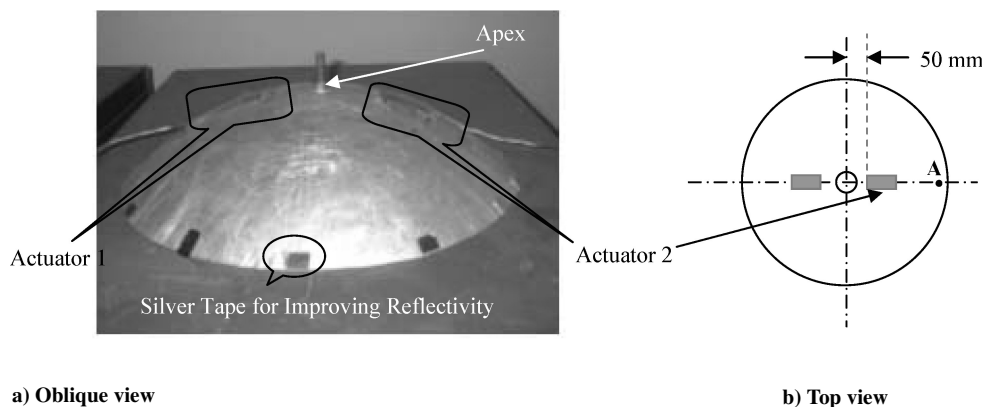


Fig. 24 Shell mounted with piezoelectric actuators.

A. Case 1: $V_A = V_B = V_C = V_D = 300$ V

Deflections along the edge AOC and BOD are plotted in Figs. 30a and 30b. From the deflection pattern, it is observed that all points A, B, C, and D are trying to move outward. Thus when the same voltage is applied to all actuators, the deformation is symmetric (outward or inward depending on $\pm V$). This type of deformation is useful in changing the coverage area of antenna (beam shaping).

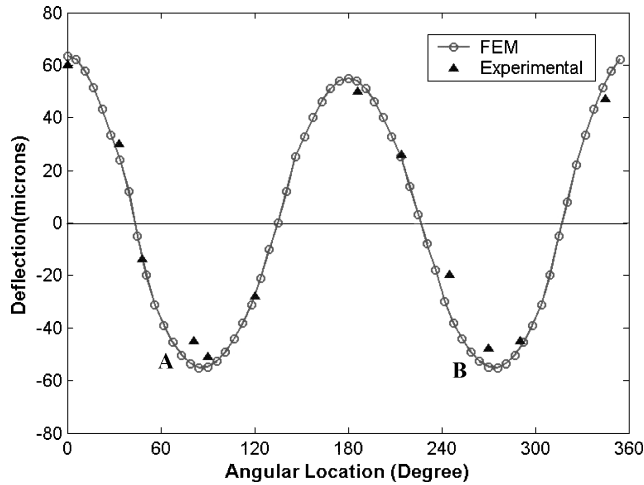


Fig. 26 Variation of deflection around the circumference of spherical shell ($V_1 = 150$ V; $V_2 = 75$ V).

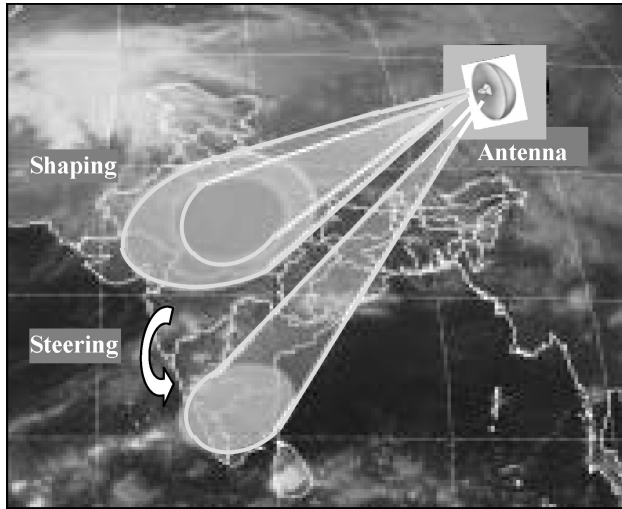


Fig. 27 Antenna shaping and steering

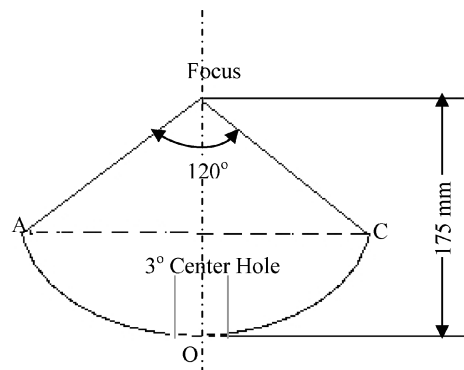
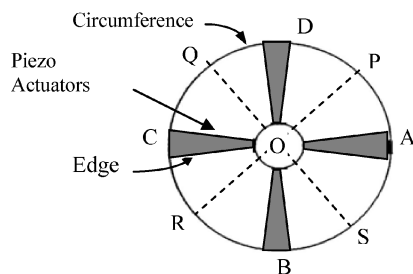


Fig. 28 Paraboloid aluminum shell structure ($t_s = 0.203$ mm, $Y_s = 0.2 \times 10^{10}$ N/m², $d_{31} = 190 \times 10^{-12}$ V/m, $t_p = 0.267$ mm, $Y_p = 0.66 \times 10^{10}$ N/m²).

B. Case 2: $V_A = V_B = 300$ V, $V_C = V_D = -300$ V

Deformation patterns along the edges AOC and BOD show similar deflection patterns (Figs. 31a and 31b). Deflection along edge POR (at 45 deg to edge AOB) is indicated in Fig. 31c. At P a deflection of -12 mm and at R a deflection of 12 mm are obtained. This is the nature of deflection required for steering, that is, changing the principal direction of propagation of antenna (beam steering). Thus

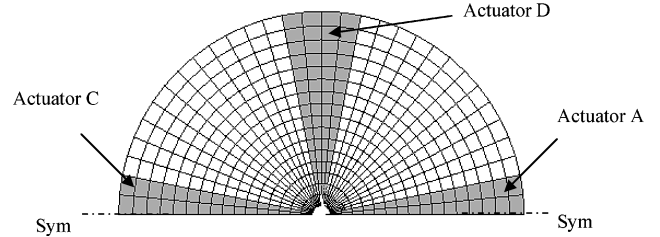
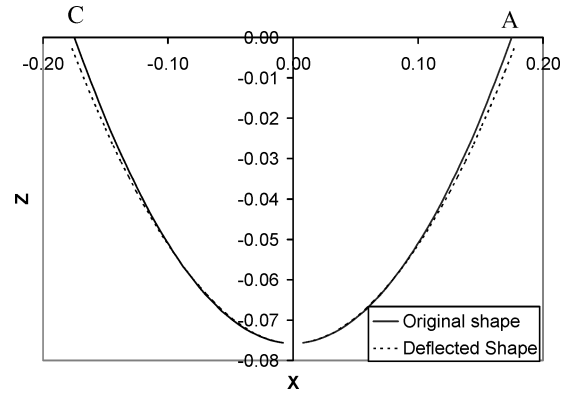
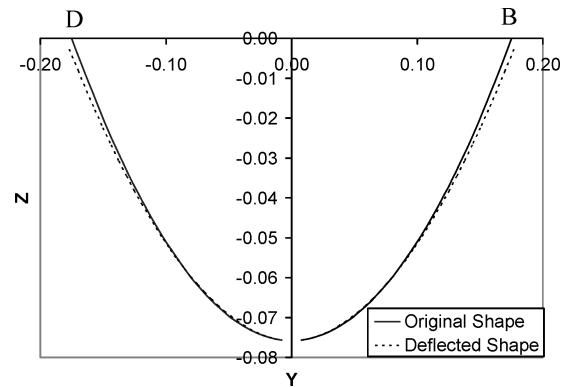


Fig. 29 Typical finite element discretization of antenna shell.



a) Deformation pattern along edge AOC



b) Deformation pattern along edge BOD

Fig. 30 Deformation pattern for $V_A = V_B = V_C = V_D = 300$ V. (Deflections are scaled by a factor of two for clarity.)

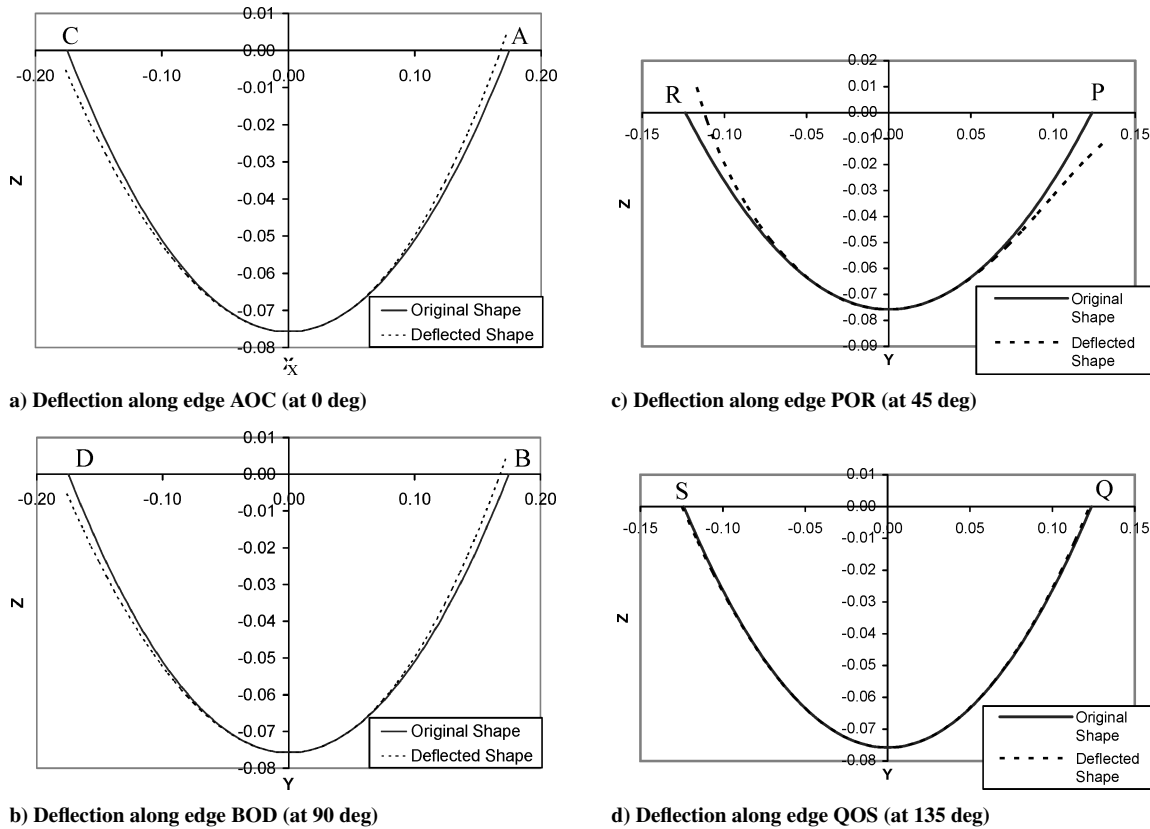


Fig. 31 Deformation pattern for $V_A = V_B = 300$ V, $V_C = V_D = -300$ V. (Deflections are scaled by a factor of two for clarity.)

piezoelectric actuators, under suitable electric field, could be used to induce desired shape changes in the antenna.

IX. Conclusions

In this paper a finite element (FE) is developed for piezoelectric actuated shell structures. It is observed that the FE formulation works well for simple beams, curved beams, and shells. Experiments conducted on different specimens have been described, and results obtained are discussed. Very good repeatability (standard deviation to mean ratio less than 5%) of the experiments is observed. It is observed that the present finite element model gives reasonably accurate prediction (less than 10% deviation) of static response to piezoelectric actuation, particularly for voltage less than half the maximum voltage. Nonlinear behavior is observed at higher voltage in almost all cases, with hysteresis of the order of 10–15%. Deviation between the finite element model and experimental results can be caused by unmodeled effects like adhesive bonding layer, hysteresis, etc., and/or variation in properties (piezoelectric coefficients, capacitance, etc.) from one actuator to another actuator and error in measurement. High electric field applied could raise the temperature of the piezomaterial leading to changes in piezoelectric coefficients.

FE predictions of the deformation pattern of a typical paraboloid smart antenna shell have been presented. It is demonstrated that deformation shapes can be induced, with suitable applied electric fields on appropriately placed actuators, which are helpful for controlling the radiation pattern, that is, beam steering and shaping. Detailed work is required to determine optimal actuator sizes, locations, and fields so as to get desired beam steering and shaping.

Acknowledgment

Authors are thankful to Department of Science and Technology, Government of India, for funding the research work.

References

- ¹Crawley, E. F., and deLuis, J., "Use of Piezoelectric Actuators as Elements of Intelligent Structures," *AIAA Journal*, Vol. 25, No. 10, 1987, pp. 1373–1385.
- ²Crawley, E. F., and Anderson, E. H., "Detailed Model of Piezoelectric Actuation of Beams," *Journal of Intelligent Material Systems and Structures*, Vol. 1, Jan. 1990, pp. 4–25.
- ³Park, C., Walz, C., and Chopra, I., "Bending and Torsion Models of Beams with Induced Strain Actuators," *Proceedings of Smart Structures and Intelligent Systems Meeting*, Vol. 1917, edited by H. W. Nesbitt, Society of Photo-Optical Instrumentation Engineers, Bellingham, WA, 1993, pp. 192–216.
- ⁴Kim, S. J., and Jones, J. D., "Optimal Design of Piezoactuators for Active Noise and Vibration Control," *AIAA Journal*, Vol. 29, No. 12, 1991, pp. 2047–2053.
- ⁵Dimitriadis, E. K., Fuller, C. R., and Rogers, C. A., "Piezoelectric Actuators for Distributed Vibration Excitation of Thin Plates," *Journal of Vibration and Acoustics*, Vol. 113, Jan. 1991, pp. 100–107.
- ⁶Tzou, H. S., "Distributed Modal Identification and Vibration Control of Continua: Theory and Applications," *Journal of Dynamic Systems, Measurement and Control*, Vol. 113, Sept. 1991, pp. 494–499.
- ⁷Tzou, H. S., and Howard, R. V., "A Piezothermoelastic Thin Shell Theory Applied to Active Structures," *Journal of Vibration and Acoustics*, Vol. 116, July 1994, pp. 295–302.
- ⁸Tzou, H. S., and Tseng, C. I., "Distributed Piezoelectric Sensor/Actuator Design for Dynamic Measurement/Control of Distributed Parameter Systems: A Piezoelectric Finite Element Approach," *Journal of Sound and Vibration*, Vol. 138, No. 1, 1990, pp. 17–34.
- ⁹Ha, S. K., Keilers, C., and Chang, F. K., "Finite Element Analysis of Composite Structures Containing Distributed Piezoelectric Sensors and Actuator," *AIAA Journal*, Vol. 30, No. 3, 1992, pp. 772–780.
- ¹⁰Hwang, W. S., and Park, H. C., "Finite Element Modeling of Piezoelectric Sensors and Actuators," *AIAA Journal*, Vol. 31, No. 5, 1993, pp. 930–937.
- ¹¹Ray, M. C., Bhattacharyya, R., and Samanta, B., "Static Analysis of an Intelligent Structure by the Finite Element Method," *Computers and Structures*, Vol. 52, No. 4, 1994, pp. 617–631.
- ¹²Chen, S. H., Wang, Z. D., and Liu, X. H., "Active Vibration Control and Suppression for Intelligent Structures," *Journal of Sound and Vibration*, Vol. 200, No. 2, 1997, pp. 167–177.

- ¹³Lam, K. Y., Peng, X. Q., Liu, G. R., and Reddy, J. N., "A Finite Element Model for Piezoelectric Composite Laminates," *Smart Materials and Structures*, Vol. 6, No. 5, 1997, pp. 583–591.
- ¹⁴Bisegna, P., and Caruso, G., "Mindlin-Type Finite Elements for Piezoelectric Sandwich Plates," *Journal of Intelligent Material Systems and Structures*, Vol. 11, No. 1, 2000, pp. 14–24.
- ¹⁵Kapania, R. K., and Mohan, P., "Static, Free Vibration and Thermal Analysis of Composite Plates and Shells Using a Flat Triangular Shell Element," *Computational Mechanics*, Vol. 17, No. 5, 1996, pp. 343–357.
- ¹⁶Kim, J., Varadan, V. V., Varadan, V. K., and Rao, X. Q., "Finite Element Modeling of a Smart Cantilever Plate and Comparison with Experiments," *Smart Materials and Structures*, Vol. 5, No. 2, 1996, pp. 165–170.
- ¹⁷Thirupathi, S. R., Seshu, P., and Naganathan, N. G., "A Finite-Element Static Analysis of Smart Turbine Blades," *Smart Materials and Structures*, Vol. 6, No. 5, 1997, pp. 607–615.
- ¹⁸Saravanos, D. A., "Mixed Laminate Theory and Finite Element for Smart Piezoelectric Composite Shell Structures," *AIAA Journal*, Vol. 35, No. 8, 1997, pp. 1327–1333.
- ¹⁹Chen, A.-H., Yao, G.-F., and Huang, C., "A New Intelligent Thin-Shell Element," *Smart Materials and Structures*, Vol. 9, No. 1, 2000, pp. 10–18.
- ²⁰Chen, S. H., Yao, G. F., and Lian, H. D., "A New Piezoelectric Shell Element and its Application in Static Shape Control," *Structural Engineering and Mechanics*, Vol. 12, No. 5, 2001, pp. 491–506.
- ²¹Balamurugan, V., and Narayanan, S., "Shell Finite Element for Smart Piezoelectric Composite Plate/Shell Structures and Its Application to the Study of Active Vibration Control," *Finite Element Analysis and Design*, Vol. 37, No. 9, 2001, pp. 713–738.
- ²²Gaudenzi, P., and Bathe, K. J., "An Iterative Finite Element Procedure for the Analysis of Piezoelectric Continua," *Journal of Intelligent Material Systems and Structures*, Vol. 6, 1995, pp. 266–273.
- ²³Lin, C. C., Hsu, C. Y., and Huang, H. N., "Finite Element Analysis on Deflection Control of Plates with Piezoelectric Actuators," *Composite Structures*, Vol. 35, No. 4, 1996, pp. 423–433.
- ²⁴Ahmad, S., Irons, B. M., and Zienkiewicz, O. C., "Analysis of Thick and Thin Shell Structures by Curved Finite Elements," *International Journal for Numerical Methods in Engineering*, Vol. 2, No. 3, 1970, pp. 419–451.
- ²⁵Benjeddou, A., "Advances in Piezoelectric Finite Element Modeling of Adaptive Structural Elements: A Survey," *Computers and Structures*, Vol. 76, No. 1–3, 2000, pp. 347–363.
- ²⁶Varadan, V. V., Chin, L., and Varadan, V. K., "Finite Element Modeling of Flexensional Electroacoustic Transducers," *Smart Materials and Structures*, Vol. 2, No. 4, 1993, pp. 201–207.
- ²⁷Yang, S. M., and Lee, Y. J., "Vibration Suppression with Optimal Sensor/Actuator Location and Feedback Gain," *Smart Materials and Structures*, Vol. 2, No. 4, 1993, pp. 232–239.
- ²⁸Shen, M.-H. H., "A New Modeling Technique for Piezoelectrically Actuated Beams," *Computers and Structures*, Vol. 57, No. 3, 1995, pp. 361–366.
- ²⁹Brennan, M. C., and McGowan, A. M. R., "Piezoelectric Power Requirements for Active Vibration Control," *Proceedings of 4th Annual Symposium on Smart Structures and Materials*, Vol. 3039, edited by V. V. Varadan and J. Chandra, Society of Photo-Optical Instrumentation Engineers, Bellingham, WA, 1997, pp. 660–669.
- ³⁰Dhage, S. D., "Strain Transfer Study in Piezoelectric Actuation of Beams," M.Tech. Dissertation, Mechanical Engineering Dept., Indian Inst. of Technology Bombay, Mumbai, India, Sept. 2000.
- ³¹Clark, R. L., Flemming, M. R., and Fuller, C. R., "Piezoelectric Actuators for Distributed Vibration Excitation of Thin Plates: A Comparison Between Theory and Experiments," *Journal of Vibrations and Acoustics*, Vol. 115, July 1993, pp. 332–339.
- ³²Gupta, V. K., Seshu, P., and Issac, K. K., "Finite Element and Experimental Studies on Piezoelectric Actuated Curved Beams," *AIAA Paper* 2002-1362, April 2002.
- ³³Panda, S. C., and Natarajan, R., "Finite Element Analysis of Laminated Composite Plates," *International Journal of Numerical Methods in Engineering*, Vol. 14, 1979, pp. 69–79.
- ³⁴MacNeal, R. H., and Harder, R. L., "A Proposed Standard Set of Problems to Test Finite Element Accuracy," *Finite Elements in Analysis and Design*, Vol. 1, No. 1, 1985, pp. 3–20.
- ³⁵Morley, L. S. D., "The Constant-Moment Plate Bending Element," *Journal of Strain Analysis*, Vol. 6, 1971, pp. 20–24.
- ³⁶MacNeal, R. H., "Specifications for the QUAD8 Quadrilateral Curved Shell Element," MacNeal-Schwendler Corp., Memo RHM-46B, Los Angeles, 1980.
- ³⁷Meirovitch, L., *Elements of Vibration Analysis*, 2nd ed., McGraw-Hill, New York, 1986, Chap. 5.
- ³⁸Yoon, H. S., and Washington, G., "Piezoceramic Actuated Aperture Antennae," *Smart Materials and Structures*, Vol. 7, No. 4, 1998, pp. 537–542.
- ³⁹Yoon, H. S., Washington, G., and Theunissen, W. H., "Analysis and Design of Doubly Curved Piezoelectric Strip-Actuated Aperture Antennas," *IEEE Transactions on Antennas and Propagation*, Vol. 48, No. 5, 2000, pp. 755–763.
- ⁴⁰Theunissen, W. H., Yoon, H. T., Burnside, W. D., and Washington, G. N., "Reconfigurable Contour Beam-Reflector Antenna Synthesis Using a Mechanical Finite-Element Description of the Adjustable Surface," *IEEE Transaction on Antennas and Propagation*, Vol. 49, No. 2, 2001, pp. 272–279.

M. Ahmadian
Associate Editor